J. Fluid Mech. (2008), *vol.* 613, *pp.* 35–53.
doi:10.1017/S0022112008003534 Printed in the United Kingdom

A new approach to understanding and modelling the influence of wall roughness on friction factors for pipe and channel flows

H. HERWIG, D. GLOSS AND T. WENTERODT

Institute for Thermo-Fluid Dynamics, Hamburg University of Technology, Denickestr. 17, 21073 Hamburg, Germany

(Received 11 December 2007 and in revised form 10 July 2008)

In this study, it is shown how the equivalent sand roughness required in the Moody chart can be calculated for arbitrarily shaped wall roughnesses. After a discussion of how to define the wall location and roughness height in the most reasonable way, a numerical approach based on the determination of entropy production in rough pipes and channels is presented. As test cases, three different two-dimensional roughness types have been chosen which are representative of regular roughnesses on machined surfaces. In the turbulent range, skin friction results with these test roughnesses can be linked to Nikuradse's sand roughness results by a constant factor. For laminar flows, a significant effect of wall roughness is identified which in most other studies is neglected completely. The dissipation model of this study is validated with experimental data for laminar and turbulent flows.

1. Introduction

Friction factors for fully developed (horizontal) pipe and channel flows are a non-dimensional representation of the pressure drop which for these flows is exactly balanced by skin friction forces. Especially for turbulent flows, they are strongly dependent on wall roughness. Since, however, the specific character of wall roughness in terms of shape, size and distribution strongly varies from case to case, an equivalent roughness of a unique character was introduced in order to enable engineers to design piping systems. This so-called *equivalent sand roughness concept* according to Moody (1944) is widely accepted as a standard approach to account for the roughness influence on skin friction factors. This classical approach to find friction factors for rough pipes or channels also involves the *hydraulic diameter concept* (see e.g. Nikuradse 1930; Schiller 1923) to account for different shapes of the cross-sections.

With these two concepts and dimensional analysis considerations, the pressure drop $\mathrm{d}p/\mathrm{d}x$ (or wall shear stress τ_w) is a function of the mean flow velocity u_m, the cross-section A with circumference C, the characteristic roughness height k, the density ϱ and the viscosity μ. It is cast into the non-dimensional form

$$f = f(Re_{Dh}, K) \tag{1.1}$$

with

$$f = -\frac{\mathrm{d}p}{\mathrm{d}x}\frac{2D_h}{\varrho u_m^2}\left(=\frac{8\tau_w}{\varrho u_m^2}\right) \qquad \text{(friction factor)}, \tag{1.2}$$

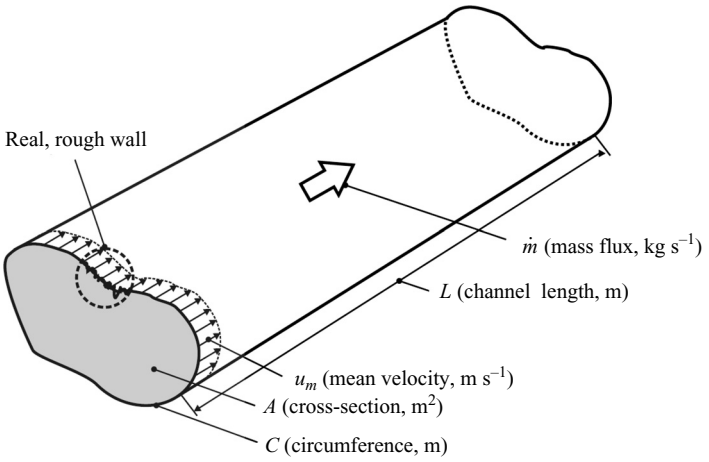

FIGURE 1. Channel of arbitrary cylindrical shape with cross-section A and length L. A, C, and u_m only apply for the equivalent smooth channel defined by D_h^e in § 4.

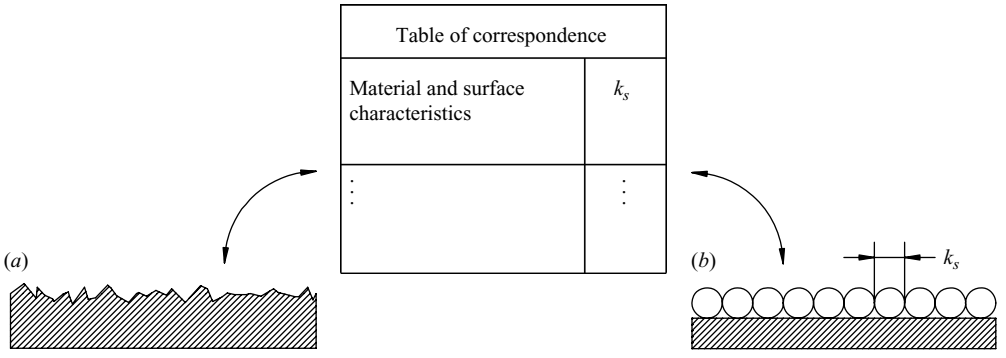

FIGURE 2. Irregular roughness (*a*) and its corresponding equivalent sand roughness (*b*).

$$Re_{Dh} = \frac{\varrho u_m D_h}{\mu} \qquad \text{(Reynolds number)}, \tag{1.3}$$

$$K = \frac{k}{D_h} \qquad \text{(roughness number)} \tag{1.4}$$

and the hydraulic diameter

$$D_h = \frac{4A}{C}. \tag{1.5}$$

The hydraulic diameter concept assumes that results gained for circular cross-sections can be used for arbitrarily shaped channels as shown in figure 1, provided D_h according to (1.5) is used as the characteristic length of the cross-section. This is an approximation which is poor for laminar flows (with deviations up to 30 %), but good for turbulent flows (with deviations often below 2 %), as shown by White (2005), for example.

The equivalent sand roughness concept assumes that each (often irregular) roughness as exemplified in figure 2(*a*) is represented by a particular homogeneous (i.e. regular) roughness which is composed of densely packed spheres of diameter k_s as shown in figure 2(*b*). This equivalent sand roughness characterized by k_s has to

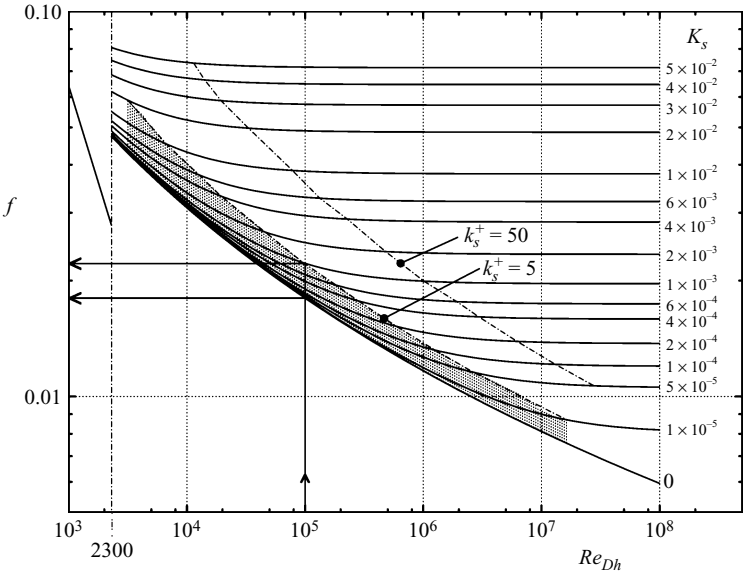

FIGURE 3. Moody chart $f(Re_{Dh}, K_s)$ for pipes; lines $k_s^+ = \text{const}$ according to (2.3); shaded area: hydraulically smooth wall ($k_s^+ < 5$).

be chosen such that f for the roughness under consideration is equal to f for the equivalent sand roughness at high Reynolds numbers, i.e. in the *fully rough flow regime*. In engineering practice, it is commonly assumed that the corresponding k_s-value is the same for all Reynolds numbers. In order to use this concept, the k_s-value of the wall roughness under consideration must be known. These corresponding values have been determined experimentally for many materials and surface finishings in the past and thus can be taken from general tables of correspondence (see e.g. table 8.1 in Munson, Young & Okiishi 2005). However, values in these tables in most cases are given as ranges, and thus provide only a low degree of accuracy.

2. The Moody chart

Figure 3 shows the famous Moody chart (see Moody 1944). Amongst others it is based on measurements by Nikuradse (1933) who was the first to study pipe flows with walls actually covered by real sand so that $k = k_s$ and $K = K_s$ (see (1.4)). According to the Moody chart, wall roughness has no effect for laminar flows ($Re_{Dh} < 2300$), i.e. $f = f(Re_{Dh})$, but has strong effects for turbulent flows ($Re_{Dh} > 2300$), i.e. $f = f(Re_{Dh}, K_s)$. For fully rough flows, the Reynolds-number dependence vanishes, i.e. $f = f(K_s)$ only.

The overall behaviour is quantified by

$$f = \frac{Po}{Re_{Dh}} \tag{2.1}$$

in the laminar range with the Poiseuille number $Po = 64$ for pipe and $Po = 96$ for channel flows (e.g. White 2005). In the turbulent range, however, the effect of Re_{Dh} and K_s on f shown in figure 3 is determined by an approximation introduced by Colebrook (1939) with the roughness number corresponding to the sand roughness

of Nikuradse's measurements. It is

$$\frac{1}{\sqrt{f}} = -2\log_{10}\left(\frac{K_s}{3.7} + \frac{2.51}{Re_{Dh}\sqrt{f}}\right). \tag{2.2}$$

The validity of this formula has been doubted ever since it was introduced (e.g. Shockling, Allen & Smits 2006; Langelandsvik, Kunkel & Smits 2008), especially in the so-called transitional regime, i.e. in the blending region between hydraulically smooth and rough pipes. Doubts especially arise, for example, when lines of $k_s^+ = \text{const}$ are included in figure 3. Here, k_s^+ is the adequate representation of wall roughness in terms of the near-wall coordinate $y^+ = yu_\tau/\nu$, with $\nu = \mu/\varrho$, i.e.

$$k_s^+ = \frac{k_s u_\tau}{\nu} \tag{2.3}$$

with the shear stress velocity $u_\tau = \sqrt{\tau_w/\varrho}$ as scaling (characteristic) velocity. As long as $k^+ < 5$ roughness elements are within the viscous sublayer, hence these walls are usually called hydraulically smooth (e.g. Schlichting & Gersten 2000) since there are no roughness effects. In the Moody chart, lines of constant k_s follow from the condition

$$k_s^+ = \frac{Re_{Dh}\sqrt{f}}{2\sqrt{2}} K_s, \tag{2.4}$$

so that the shaded area in figure 3 can be identified as one where the wall actually is hydraulically smooth. The Moody chart differs from this, however. Take, for example, the friction factor for $Re_{Dh} = 10^5$ and $k_s^+ = 5$ which is 23 % higher than that of a smooth wall.

3. The dissipation model approach

Losses within internal flows are often named *pressure losses*; however, they should more accurately be called *losses of total head* since they occur when the total pressure, i.e. the mechanical energy in a flow, is reduced. In such a process, mechanical energy is converted into internal energy (conserving the total energy in accordance with the first law of thermodynamics). In thermodynamics, this is a dissipation process (dissipation of mechanical energy), so that a non-zero friction factor f is due to finite dissipation rates in the flow.

Turning this argument around, an alternative approach is straightforward: we can determine the local dissipation rates in the flow, integrate them over the flow domain and thus find the corresponding friction factor. If this is done within the precise geometry, i.e. including the details of the rough wall, $f = f(Re_{Dh}, K)$ can be found with K as a non-dimensional representation of the actual wall roughness.

First, however, we discuss the problem of D_h- and k-values for rough walls, since D_h and k are required for f, Re_{Dh} and K, even in the dissipation model approach.

4. A misleading question: where is the wall?

In view of the surface profile of a rough wall the question arises: where actually is the wall? The answer to this question, however, is strikingly simple: the wall is where it is, and it is a rough wall. This question is better phrased as: where is the equivalent smooth wall with respect to the real rough wall? This equivalent wall and the equivalent channel, respectively, define D_h in f and Re_{Dh} according to (1.2) and (1.3). Therefore, this hydraulic diameter will be called D_h^e hereinafter

(e for equivalent). The question with respect to D_h^e, however, can only be answered in relation to an *equivalence criterion*, from which in turn it can be decided which smooth wall representation is equivalent to the real rough wall.

Three choices (with the first and the third of them often used) are:

(i) D_{hI}^e: D_h as a certain geometrical mean value based on assumptions about the physics of the flows around the roughness elements (e.g. Croce & D'Agaro 2005; Hu, Werner & Li 2004; Kleinstreuer & Koo 2004; Kandlikar *et al.* 2005).

(ii) D_{hII}^e: D_h for which the law for the smooth wall $f(Re_{Dh}, K=0)$ also holds for $K \neq 0$.

(iii) D_{hIII}^e: D_h such that the volume V of the real channel is equal to the corresponding volume $V = A(D_{hIII}^e)L$ of the equivalent smooth channel where A is evaluated with D_{hIII}^e (e.g. Nikuradse 1933).

From our point of view, D_h^e should be such that it can be measured without access to the surface, i.e. without opening the channel. This would be an *operational definition* of D_h^e. Furthermore, the mean velocity $u_m \equiv \dot{m}/\varrho A(D_h^e)$ should be $u_m = \dot{m}L/m = \dot{m}L/\varrho V$ with $\dot{m}$ being the mass flux, V the volume of the real channel and m the mass of the fluid inside of it. Then, the real volume V is the only information we require, provided $\dot{m}$ is known. Both constraints are met by $D_h^e = D_{hIII}^e$ only. With $\dot{m}$ and V we obtain

$$D_h^e = \frac{4V}{C\left(D_h^e\right)L}, \tag{4.1}$$

$$u_m = \frac{\dot{m}L}{\varrho V}. \tag{4.2}$$

The real volume V can be determined by measuring how much fluid it takes to fill the rough channel, as Nikuradse (1933) did.

In (4.1), $C(D_h^e)$ is the circumference of the equivalent smooth channel. Its shape has to be determined under the constraint that the resulting volume is that of the real channel, i.e. V. There are two options to achieve this. Either the cross-sectional form (circular, triangular, plane channel, ...) is preset or an equivalence criterion (least standard deviation, ...) is defined with some smoothness condition to be met. Setting a circular cross-section, for example, $C = \pi D_h^e$ and therefore $D_h^e = 2\sqrt{V/\pi L}$ from (4.1).

With D_h^e and u_m according to (4.1) and (4.2), respectively, the friction law for rough pipes can be cast into the well-known form $f(Re_{Dh}, K)$ defined in (1.1)–(1.4).

5. An open question: how to define the roughness parameter?

Now that D_h has been defined in the previous section (hereinafter, we omit the index e), the next question is what is the appropriate definition of the roughness parameter k that goes into the roughness number K according to (1.4). There are different concepts of how to define the overall effect of wall roughness. Three such concepts, each with its own definition of a roughness parameter k, are:

(i) k_I: A particular roughness is characterized by its own parameter k_I. The influence of this kind of wall roughness is determined for different values of k_I. These results, however, cannot be transferred to other kinds of roughness.

(ii) k_{II}: A general definition of k is sought by which there is a unique representation of different kinds of roughness which has to be determined once for different values of k_{II}.

(iii) k_{III}: A uniform kind of roughness is defined as a standard roughness with a roughness parameter k_{III}. Its influence is determined once for different values

of k_{III}. All other kinds of roughness are individually referred to this case. The equivalent standard roughness is determined case by case and stored in a table of correspondence.

We easily recognize k_{III} as the equivalent sand roughness concept which has been widely used so far. Its shortcoming is the need for a table of correspondence which provides a very rough estimate only.

k_{II} would be an appealing alternative. There are doubts, however, whether such a unique parameter k_{II} exists, since the problem presumably is a multi-parameter problem. Nevertheless, there have been many attempts in this direction (e.g. Kandlikar *et al.* 2005).

The individual determination of k_I is obviously the most straightforward approach; but it also is the least attractive one, since it just puts on record what is measured without any generality in applying these results.

Whatever the choice between k_I, k_{II} and k_{III}, we must determine the influence of wall roughness on the loss of total pressure. This can be done experimentally (as in the past) or by analysing the dissipation process with an analytical/numerical approach which we want to present here.

6. Dissipation model details

Dissipation of mechanical energy from a thermodynamic point of view is directly linked to the production of entropy in a flow field. Therefore, a thermodynamic second law analysis can give valuable information about losses in flows (see Rosen 1998; Hesselgreaves 2000; Wang *et al.* 2003). The entropy production occurs locally in the presence of velocity gradients. Mathematically, it is represented by one term in the balance equation for entropy. For Newtonian fluids, the specific entropy production rate in Cartesian coordinates with T as thermodynamic temperature is (see Bejan 1996; Herwig & Kautz 2007)

$$\dot{S}'''_D = \frac{\mu}{T}\left(2\left[\left(\frac{\partial u}{\partial x}\right)^2+\left(\frac{\partial v}{\partial y}\right)^2+\left(\frac{\partial w}{\partial z}\right)^2\right] + \left(\frac{\partial u}{\partial y}+\frac{\partial v}{\partial x}\right)^2+\left(\frac{\partial u}{\partial z}+\frac{\partial w}{\partial x}\right)^2+\left(\frac{\partial v}{\partial z}+\frac{\partial w}{\partial y}\right)^2\right), \quad (6.1)$$

and can be evaluated once the flow field (u, v, w) is known in detail.

For turbulent flows with a RANS approach (Reynolds averaged Navier–Stokes), $\dot{S}'''_D$ is a time-averaged term with two parts: one represents the entropy production due to the time averaged velocity and one is a result of velocity fluctuations. This partitioning is somewhat arbitrary, but follows the general idea of the RANS approach. These turbulent terms are (see Kock & Herwig 2004; Herwig & Kock 2007), with $\dot{S}'''_D = \dot{S}'''_{\overline{D}} + \dot{S}'''_{D'}$

$$\dot{S}'''_{\overline{D}} = \frac{\mu}{\overline{T}}\left(2\left[\left(\frac{\partial \overline{u}}{\partial x}\right)^2+\left(\frac{\partial \overline{v}}{\partial y}\right)^2+\left(\frac{\partial \overline{w}}{\partial z}\right)^2\right] + \left(\frac{\partial \overline{u}}{\partial y}+\frac{\partial \overline{v}}{\partial x}\right)^2+\left(\frac{\partial \overline{u}}{\partial z}+\frac{\partial \overline{w}}{\partial x}\right)^2+\left(\frac{\partial \overline{v}}{\partial z}+\frac{\partial \overline{w}}{\partial y}\right)^2\right), \quad (6.2)$$

$$\dot{S}'''_{D'} = \frac{\mu}{\overline{T}}\left(2\left[\overline{\left(\frac{\partial u'}{\partial x}\right)^2} + \overline{\left(\frac{\partial v'}{\partial y}\right)^2} + \overline{\left(\frac{\partial w'}{\partial z}\right)^2}\right] + \overline{\left(\frac{\partial u'}{\partial y} + \frac{\partial v'}{\partial x}\right)^2} + \overline{\left(\frac{\partial u'}{\partial z} + \frac{\partial w'}{\partial x}\right)^2} + \overline{\left(\frac{\partial v'}{\partial z} + \frac{\partial w'}{\partial y}\right)^2}\right). \quad (6.3)$$

Since results of calculations based on the RANS approach will provide mean velocity components $\overline{u}$, $\overline{v}$ and $\overline{w}$ but not the fluctuating velocity components, $\dot{S}'''_{\overline{D}}$ can be evaluated but $\dot{S}'''_{D'}$ cannot.

The physics behind $\dot{S}'''_{D'}$ is the so-called turbulent dissipation. This part of the total dissipation is basically contained in the quantity ε introduced in most turbulence models. Here, 'basically' means that ε exactly corresponds to $\dot{S}'''_{D'}$ only in the asymptotic limit $Re_{Dh} \to \infty$, as shown in Kock & Herwig (2004) and Mathieu & Scott (2000). For finite Reynolds numbers, it is an (asymptotic) approximation replacing (6.3) by

$$\dot{S}'''_{D'} = \frac{\varrho\varepsilon}{\overline{T}}, \quad (6.4)$$

where ε comes from the model equation for ε in the k–ε turbulence model, for example.

With $\dot{S}'''_D$ according to (6.1) for laminar flows and $\dot{S}'''_D = \dot{S}'''_{\overline{D}} + \dot{S}'''_{D'}$ for turbulent flows, the local entropy production rate can be determined when u, v, w or $\overline{u}, \overline{v}, \overline{w}$ and ε distributions are known in the whole flow field, respectively. This means that the method is a post-processing step, imposing no additional cost to the calculation itself. Integration with respect to the channel volume V gives the overall entropy production rates

$$\dot{S}_D = \int_V \dot{S}'''_D \,\mathrm{d}V, \qquad \dot{S}_{\overline{D}} = \int_V \dot{S}'''_{\overline{D}} \,\mathrm{d}V, \qquad \dot{S}_{D'} = \int_V \dot{S}'''_{D'} \,\mathrm{d}V. \quad (6.5)$$

In channel flows, they immediately provide the specific energy dissipation rate between two cross-sections 1 and 2 in terms of

$$\varphi_{12} \equiv T\dot{S}_D\big|_{12}/\dot{m} \qquad \text{(laminar flow)}, \quad (6.6)$$

$$\varphi_{12} \equiv \overline{T}\left(\dot{S}_{\overline{D}}\big|_{12} + \dot{S}_{D'}\big|_{12}\right)/\dot{m} \qquad \text{(turbulent flow)}, \quad (6.7)$$

assuming constant density ϱ. From φ_{12}, we find the friction factor in a more general form than in § 1, cf. (1.2),

$$f_{12} \equiv \frac{\varphi_{12}}{L_{12}}\frac{2D_h}{u_m^2} \quad \text{or} \quad f \equiv \frac{\mathrm{d}\varphi}{\mathrm{d}x}\frac{2D_h}{u_m^2}, \quad (6.8)$$

where L_{12} is the distance between the cross-sections 1 and 2. Here, f_{12} and f are a global and a local value, respectively.

For the special case of a fully developed flow (i.e. no changes in streamwise velocity profiles) flowing horizontally (i.e. no changes in potential energy), φ_{12} is immediately linked to the pressure drop, i.e.

$$\varphi_{12} = -\frac{p_2 - p_1}{\varrho} \quad \text{(laminar)}, \quad \varphi_{12} = -\frac{\overline{p_2} - \overline{p_1}}{\varrho} \quad \text{(turbulent)}. \quad (6.9)$$

This is why f according to (6.8) is often written in terms of $\mathrm{d}p/\mathrm{d}x$ or τ_w, since, for fully developed horizontal flows,

$$f \equiv \frac{\mathrm{d}\varphi}{\mathrm{d}x}\frac{2D_h}{u_m^2} = \underbrace{-\frac{\mathrm{d}p}{\mathrm{d}x}\frac{2D_h}{\varrho u_m^2} = \frac{8\tau_w}{\varrho u_m^2}}_{\text{Fully developed, horizontal}}. \tag{6.10}$$

The general definition (6.8) of a friction factor f_{12} or f representing losses of mechanical energy (in thermodynamic, losses of exergy or available work) is still applicable when the flow is transient, not fully developed or undergoes changes in potential energy. For example, f according to (6.8) can be introduced for a radial and thus decelerated channel flow, but for this case can be linked to neither $\mathrm{d}p/\mathrm{d}x$ nor τ_w, because they are not representative of losses of total pressure (and thus for losses of mechanical energy).

To illustrate the dissipation model, consider the friction factor according to (6.8) for the fully developed laminar flow in a horizontal plane channel with smooth walls. Between the two walls of distance $2H$ the velocity profile is (see White 2005)

$$u = \tfrac{3}{2}u_m\left[1-\left(\frac{y}{H}\right)^2\right] \tag{6.11}$$

when y starts from the centreline. Substituting this velocity in (6.1) and evaluating $\dot{S}_D$, φ_{12} and f_{12}, f according to (6.5), (6.6) and (6.8), respectively, results in

$$f_{12} = f = \frac{32}{Re_{Dh}}\int_0^1\left(\frac{\partial u/u_m}{\partial y/H}\right)^2 \mathrm{d}(y/H) = \frac{96}{Re_{Dh}}, \tag{6.12}$$

confirming that $Po = 96$ for the plane channel, cf. (2.1). For more complicated geometries, integration must be performed numerically. For rough walls, this includes all fluid-filled cavities.

7. Advantages of the dissipation model

Since the overall dissipation between two cross-sections in fully developed horizontal channel flow, φ_{12} according to (6.9), basically is $p_2 - p_1$ and $\overline{p_2} - \overline{p_1}$, respectively, one might argue that, especially in a numerical approach to the problem, it is sufficient merely to determine the pressure in the two cross-sections 1 and 2.

As mentioned already, this is only true for the special case of a steady fully developed horizontal flow. Only then are changes in pressure equivalent to changes in total pressure and thus can be taken as losses. Whenever there is a flow development in a channel or a flow through a non-cylindrical geometry, $p_2 - p_1$ does not correspond to φ_{12} and the general dissipation model approach is required in order to determine f_{12} or f according to (6.8).

Also, the general advantage holds that a quantity following from integrating a field variable is more accurate than one that follows from the difference of two quantities $(p_2 - p_1)$ or the gradient of one quantity $(\tau_w = \mu(\partial u/\partial y)_w)$.

However, even for the case of fully developed horizontal flows, our dissipation model allows a look into the 'black box of $f_{12} = -(p_2 - p_1)2D_h/\varrho L_{12}u_m^2$'. The detailed entropy production field yields information about where and how losses occur. This information is the background for a physical interpretation as well as for systematic modifications of wall roughness, for example in heat transfer problems.

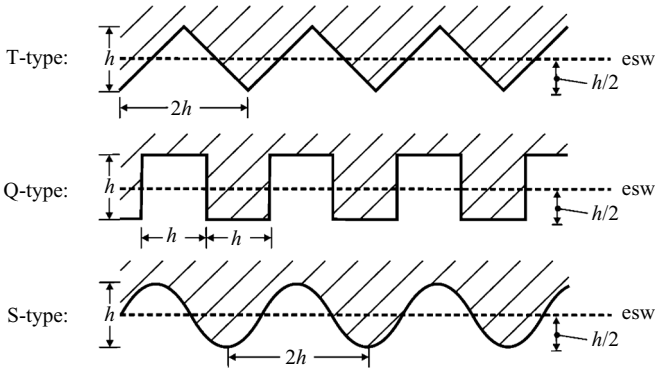

FIGURE 4. Three types of regular roughness elements (esw: equivalent smooth wall; for the definition of $D_h = D^e_{hIII}$, see § 4). Note: the position of esw indicated above is that for plane channels.

8. Application of the dissipation model

In this study, we apply the dissipation model in a two-dimensional and an axisymmetric version, representing a channel and a pipe flow, respectively. Such two-dimensional roughness contours are representative of the regular roughnesses on machined surfaces such as honed pipes. Their increasing application in engineering causes a demand for deeper analysis of the roughness effects (e.g. Sletfjerding, Gudmundsson & Sjøen 1998; Shockling *et al.* 2006).

The fluid is considered to be Newtonian. Since thermal effects due to dissipation of mechanical energy are negligible in most technical applications, the flow is considered to be isothermal. As far as wall roughness is concerned, roughness elements then are grooves in the wall, perpendicular to the streamwise direction. According to the equivalent sand roughness concept, rough walls of this special kind are related to a certain sand roughness height k_s. For our calculations, we use three types of regular roughness elements shown in figure 4: triangular (T-type), quadratic (Q-type) and sinusoidal (S-type) roughness with the characteristic length scale h.

We systematically vary the roughness height $k_I \equiv h$ in equal steps as

$$K_I = \frac{k_I}{D_h} = 0, 0.005, \ldots, 0.05 \text{ (laminar)}, \qquad K_I = 0, 0.005, \ldots, 0.025 \text{ (turbulent)}. \tag{8.1}$$

Here, k_I is an individual roughness parameter which, later on, must be linked to the standard roughness parameter $k_{III} = k_s$, as discussed in § 5.

Since the flows under consideration are quasi-fully developed (velocity changes only on a length scale $\Delta x = O(h)$, periodically repeated downstream) we can set periodic boundary conditions on a section of the whole flow field shown in figure 5(*a*) for the S-type rough wall. The numerical grids shown in figure 5(*b*) consist of two-dimensional three-knot triangular elements locally refined towards the wall. In order to guarantee grid-independent solutions, calculations were performed with at least two different grid refinements and accepted only when deviations in the solutions on two different grids were less than 0.1 %.

When dissipation rates φ_{12} according to (6.6) and (6.7) are determined, the actual length is $L_{12} = 2h$ and therefore φ_{12} is the specific dissipation rate in the section of the flow field that is covered by the numerical grid.

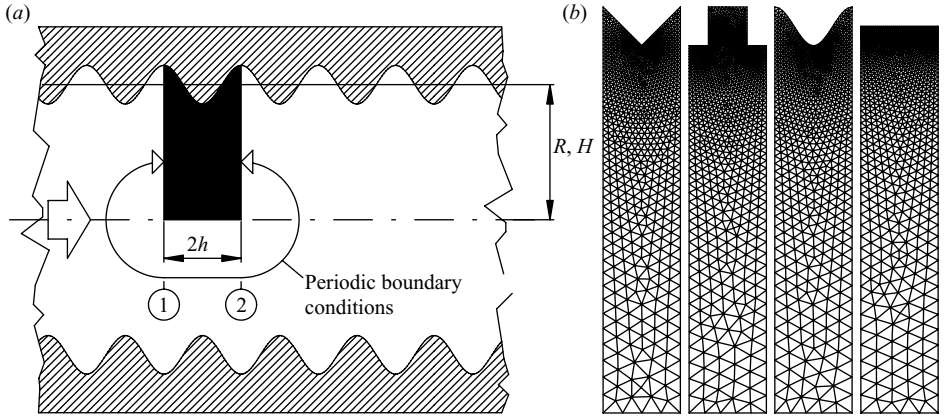

FIGURE 5. Details of the numerical solution: (*a*) solution domain with periodic boundary conditions; (*b*) numerical grid (three-knot triangular elements) for the three types of roughness and for the smooth wall.

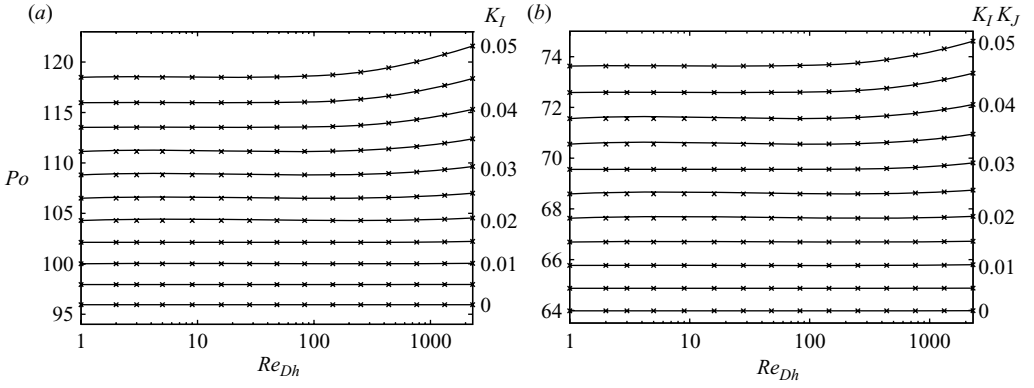

FIGURE 6. Poiseuille number for laminar flows and T-type wall roughness. (*a*) Channel flow (*b*) Pipe flow.

8.1. *Laminar flows*

For laminar flows, cf. (6.6),

$$\dot{m}\varphi_{12} = T\dot{S}_D\big|_{12} = \mu \int \left(2\left[\left(\frac{\partial u}{\partial x}\right)^2 + \left(\frac{\partial v}{\partial y}\right)^2 \right] + \left(\frac{\partial v}{\partial x} + \frac{\partial u}{\partial y}\right)^2 \right) \mathrm{d}V \qquad (8.2)$$

must be determined numerically in the solution domain for the plane channel, and the corresponding form for the axisymmetric pipe flow. The CFD code FLUENT6.3 is used to solve the steady laminar Navier–Stokes equations (incompressible and isothermal).

Figure 6 shows results in terms of $Po(Re_{Dh}, K_I)$ for the T-type roughness in channels and pipes. Each symbol $\times$ corresponds to a calculated case, full lines are added to connect cases with the same K_I-value. Two features are obvious:

(i) There is an influence of wall roughness on Po or f. With $K_I = 0.05$ it is about 23 % for the channel flow and about 15 % for the pipe flow.

(ii) Po is independent of Re_{Dh} for $Re_{Dh} \to 0$ and for $K_I \to 0$ since in both limits the convective terms (inertia forces) in the Navier–Stokes equations vanish. For

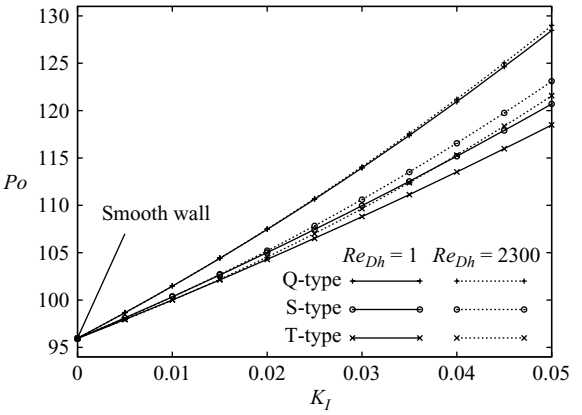

FIGURE 7. Poiseuille number of the channel flow as a function of K_I (wall roughness) for two Reynolds numbers Re_{Dh}.

large Re_{Dh} and K_I, however, convective terms are relevant (since neither $v=0$ nor $\partial u/\partial x=0$ holds close to the rough wall).

The overall effect is shown in figure 7 for the channel flow at two Reynolds numbers ($Re_{Dh}=1$ and 2300). The curves are interpolations with respect to the calculated values. Obviously the Q-type roughness elements have the strongest effect with an increase in Po of almost 34 % for $K_I=0.05$ followed by the S- and T-type. The influence of Re_{Dh} on Po, however, is lowest for the Q-type roughness.

The distribution of the entropy production is shown in figure 8 for all three types of wall roughness at two different Reynolds numbers ($Re_{Dh}=145$ and 2300). A common feature of all three geometries is that almost no entropy production occurs in the cavities between the elements, but it is rather concentrated in a small band along the heads of the single roughness elements. While for $Re_{Dh}=145$ the areas of equal entropy production show a pattern of symmetry, this symmetry is disturbed for higher Reynolds numbers owing to the influence of the convective terms.

The decreasing roughness effect (in the order Q-, S-, T-type) obviously corresponds to the decreasing percentage of a nearly horizontal wall in the small band of high entropy production. For the Q-type it is 50 %, for the S-type ≈ 20 % and for T-type almost zero.

8.2. *Turbulent flows*

For turbulent flows, cf. (6.7),

$$\overline{T}\,\dot{S}_{\overline{D}}\big|_{12} = \mu \int \left(2\left[\left(\frac{\partial \overline{u}}{\partial x}\right)^2 + \left(\frac{\partial \overline{v}}{\partial y}\right)^2 \right] + \left(\frac{\partial \overline{v}}{\partial x} + \frac{\partial \overline{u}}{\partial y}\right)^2 \right) \mathrm{d}V, \tag{8.3}$$

$$\overline{T}\,\dot{S}_{D'}\big|_{12} = \varrho \int \varepsilon \mathrm{d}V, \tag{8.4}$$

have to be calculated for two-dimensional channel flows, for example.

We use FLUENT6.3 now for the calculation of the turbulent flow field (incompressible, isothermal), with the k–ε RNG turbulence model by Yakhot & Orszag (1986) in the RANS approach. From these results, we find f according to (6.8). Figure 9 shows our results in terms of $f(Re_{Dh}, K_I)$ for pipes. Again each symbol $\times$ corresponds to a calculated case and full lines are added to connect cases with the same K_I-value.

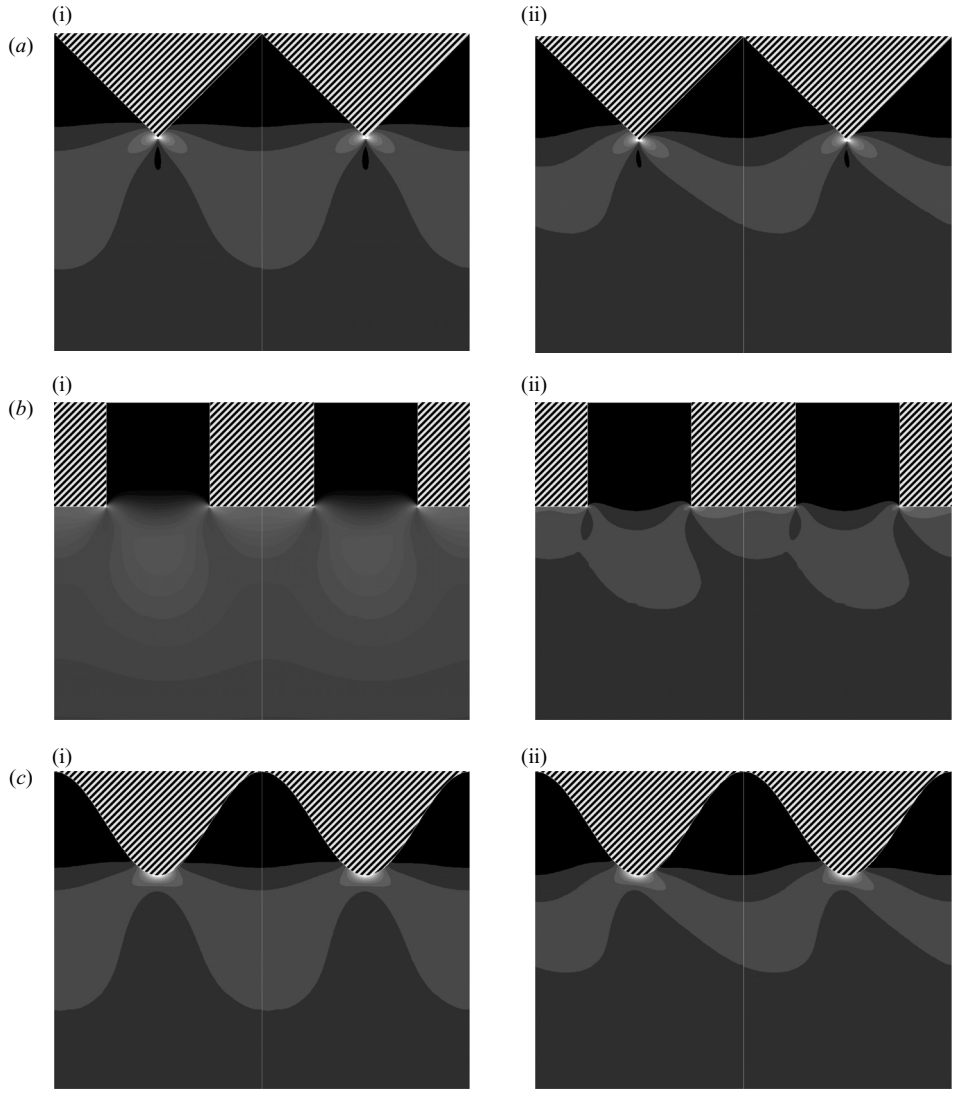

FIGURE 8. Distribution of the specific entropy production rate $\dot{S}'''_D$. Close-up of the rough wall for two Reynolds numbers (dark: weak; light: strong; equal grey scales within each Reynolds number only), laminar flow: (*a*) T-type wall roughness; (*b*) Q-type wall roughness and (*c*) S-type wall roughness. (i) $Re_{Dh} = 145$; (ii) $Re_{Dh} = 2300$.

The dotted lines are calculated according to Colebrook's formula (2.2) with roughness numbers K_s different from our K_I numbers. The K_s numbers are chosen such that all f-values according to (2.2) at $Re_{Dh} = 10^8$ are equal to the f-values resulting from our simulations at $Re_{Dh} = 10^8$. Our roughness numbers are $K_I = h/D_h$ and are related to Colebrook's K_s numbers as shown in figure 13.

Important aspects that can be seen in figure 9 are:

(i) Curves $k^+ = 5$ (here indicated by symbol $\odot$) are close to those for $k^+ = 0$ (smooth wall, here shown for $Re_{Dh} < 10^6$) indicating that for $k^+ < 5$, the wall is hydraulically smooth, cf. figure 3 and the discussion with respect to the shaded area in it.

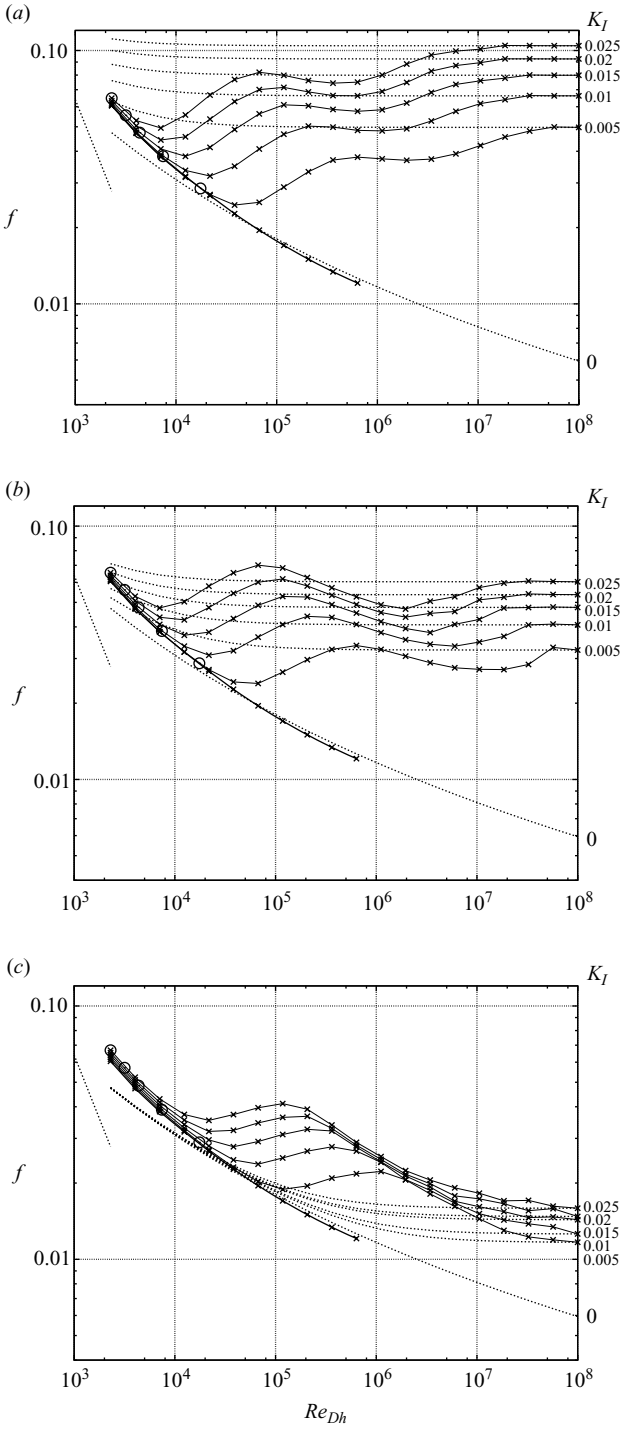

FIGURE 9. Friction factor for turbulent pipe flow; $\odot$: $k^+ = 5$ according to (2.4). (*a*) T-type wall roughness. (*b*) S-type wall roughness. (*c*) Q-type wall roughness.

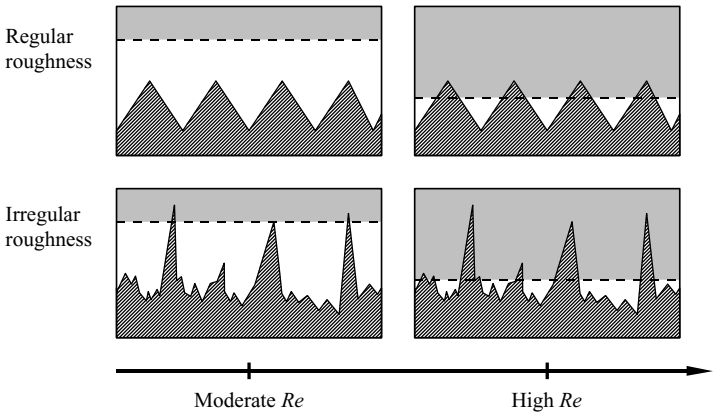

FIGURE 10. Decreasing height of the viscous sublayer with increasing Reynolds numbers and the intrusion of regular and irregular roughnesses into it (dashed line: 'edge' of the viscous sublayer).

(ii) As in the Moody chart, f becomes independent of Re_{Dh} for $Re_{Dh} \to \infty$ for the T- and S-type roughness. The physical explanation for that behaviour is a total destruction of the viscosity-dominated wall layer by large roughness elements.

(iii) For the Q-type roughness, the Re_{Dh}-dependence does not vanish with high Re_{Dh}-numbers, instead the lines for $K_I > 0$ behave as the line $K_I = 0$. This behaviour of the Q-type roughness was first systematically investigated by Perry, Schofield & Joubert (1969) who called it 'd' type roughness because the respective equivalent sand roughness is not proportional to k_I, but to a boundary-layer thickness d.

(iv) In the Moody chart, the curve $f(Re_{Dh}, K_s)$ for $K_s = \text{const}$ decreases monotonically between the two limits of small and large Reynolds numbers. Our curves $f(Re_{Dh}, K_I)$, however, have a distinct minimum close to the curve for smooth walls ($K_I = K_s = 0$). This *inflectional behaviour* can be found in all studies on regular roughnesses (e.g. Schiller 1923; Nikuradse 1933; Streeter 1936). It was also discussed in Schlichting (1965) and in Bradshaw (2000) and can be traced back to the uniformity of roughness elements. Nikuradse had to accept small deviations from a particular sand grain size owing to imperfect sieving, whereas in our numerical approach, the deviation is zero by definition, yielding a larger range of Reynolds numbers where the deviation from a monotonic behaviour occurs.

Obviously, regarding the departure from the smooth wall, the effects of regular surface roughnesses differ from that of irregular surface roughnesses for increasing Reynolds numbers. One possible explanation for this is illustrated in figure 10. Whereas a regular roughness sticks out of the viscous sublayer for high Reynolds numbers, it may not do this for moderate Reynolds numbers (and thus shows a smooth wall behaviour). An irregular roughness, however, may for all Reynolds numbers behave differently from the smooth-wall case because certain elements always stick out of the viscous sublayer. Therefore the transition between moderate and high Reynolds numbers can be smooth for irregular roughnesses, but more or less abrupt or even non-monotonic for regularly rough walls.

In figure 11, the distribution of entropy production between $\dot{S}_{D'}$ and $\dot{S}_{\overline{D}}$ is shown for all three types of wall roughness. According to these results, turbulent dissipation becomes dominant for $Re_{Dh} \to \infty$, i.e. in the range of fully turbulent flows for which $f = f(K)$ only (except for 'd' type roughnesses as in our Q-type test case). This also may explain why f becomes independent of Re_{Dh} for $Re_{Dh} \to \infty$. The dissipation

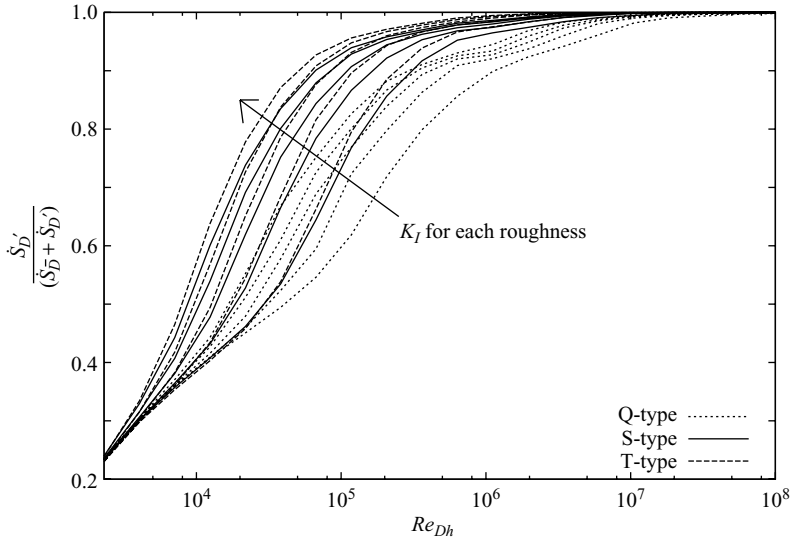

FIGURE 11. Details of the entropy production distribution for all three types of wall roughness.

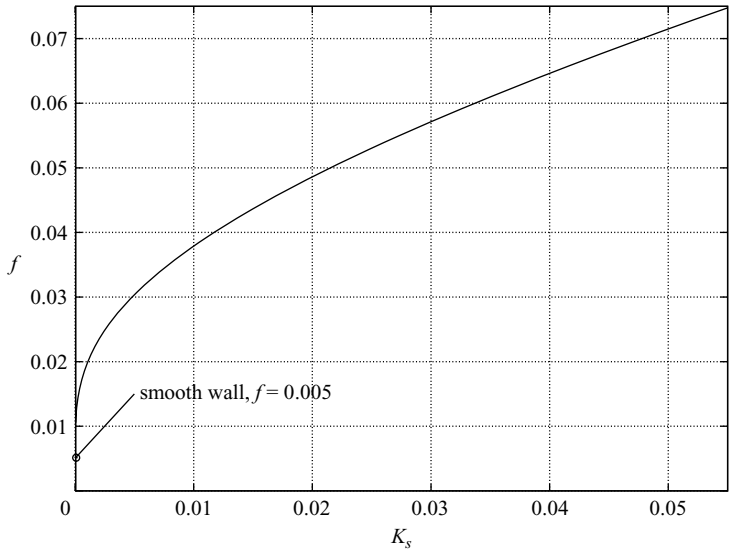

FIGURE 12. Friction factor of the channel flow as a function of K_s (wall roughness) for $Re_{Dh} = 10^8$ according to (2.2).

part $\dot{S}_{\overline{D}}$ vanishes; this part, however, is Re_{Dh}-dependent through the way in which the time mean velocity profile changes with Re_{Dh}.

Figure 12 shows that the effect of wall roughness in turbulent flows is qualitatively different from that in laminar flows (cf. figure 7). In laminar flows there is an almost linear increase of $f = Po/Re_{Dh}$ with K_I according to our results, whereas it is highly nonlinear for turbulent flows according to (2.2).

As another consequence of the different wall roughness impact in the laminar and turbulent regime, the concept of an equivalent sand roughness which is well-established for fully turbulent flows cannot be extended to laminar flows with the same values of K_s for both flow regimes. Furthermore, even the sequence of roughness

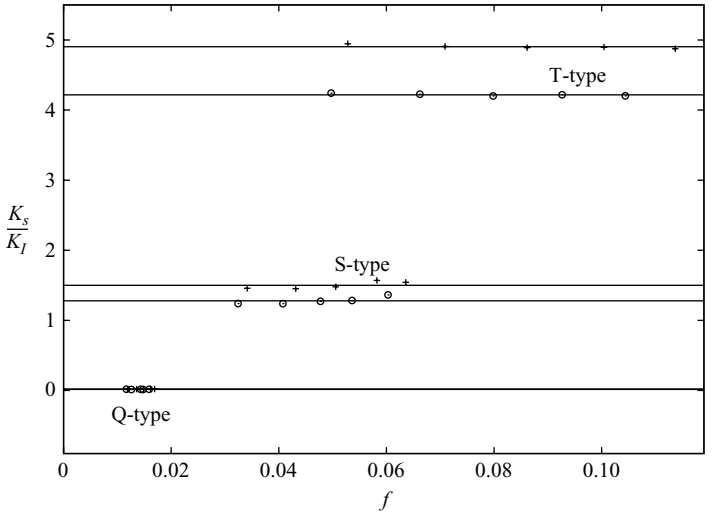

FIGURE 13. Correlation of roughness numbers K_s and K_I. +, plane channel; ∘, pipe.

types with respect to an increase in impact is different: it is T/S/Q for laminar flows (cf. figure 7), but Q/S/T for turbulent flows (cf. figure 9*a–c*).

The important relation of our roughness number $K_I = h/D_h$ and K_s in the Moody chart can best be expressed in terms of K_s/K_I as a function of f for Reynolds numbers high enough that $f = f(K_s)$ and $f = f(K_I)$, respectively. Figure 13 shows there is a linear dependence of K_I and K_s, i.e. $K_s = \text{const} \times K_I$. As a consequence for each kind of roughness, characterized by one geometric parameter $k = k_t$, one calculation based on our dissipation model will give the fixed ratio $k_s/k_t = K_s/K_t$ with k_s as equivalent sand roughness height. Here, the index t stands for technical roughness. When K_s/K_t has been determined, the Moody chart can subsequently be used for that roughness. Thus numerical calculations can replace an experimentally determined table of correspondence.

9. Validation of the dissipation model

In order to validate the dissipation model of this study, we compare experimental data for pipe and channel flows to the corresponding results gained by our theoretical approach. We do this for two types of flow. One is the laminar radially outward flow between two disks with one smooth and one rough wall by Gloss, Dittmer & Herwig (2008); the other flow is the fully developed turbulent pipe flow with rough walls by Schiller (1923).

(i) In Gloss *et al.* (2008), two disks of the size of silicon wafers are brought close together with a flow between them from the centre to the edge. One disk is actually a silicon wafer with a Q-type roughness of size $k_I = h = 20\,\mu\text{m}$ (cf. figure 4) etched into it. If now the disk clearance $D_h/2$ is changed continously the relative roughness $K = h/D_h$ can be changed without touching the roughness itself. Figure 14 shows the effect of surface roughness in terms of the pressure drop with one rough wall compared to the case with both walls being smooth.

For two Reynolds numbers at the inlet ($Re = 17$ and 175), measurements are compared to the results of a numerical calculation based on the dissipation model for laminar flows. There is a good agreement and thus verification that there is also an influence of rough walls in laminar flows.

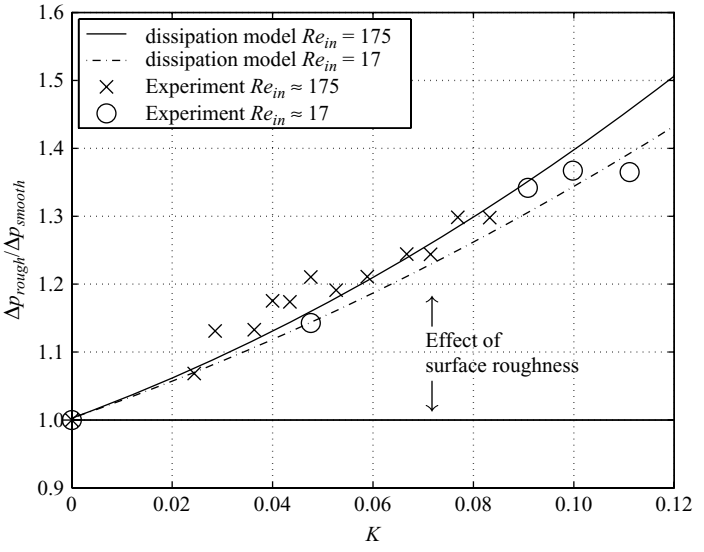

FIGURE 14. Experimental data and numerical results for an increasing roughness number of a laminar flow between two disks, taken from Gloss *et al.* (2008).

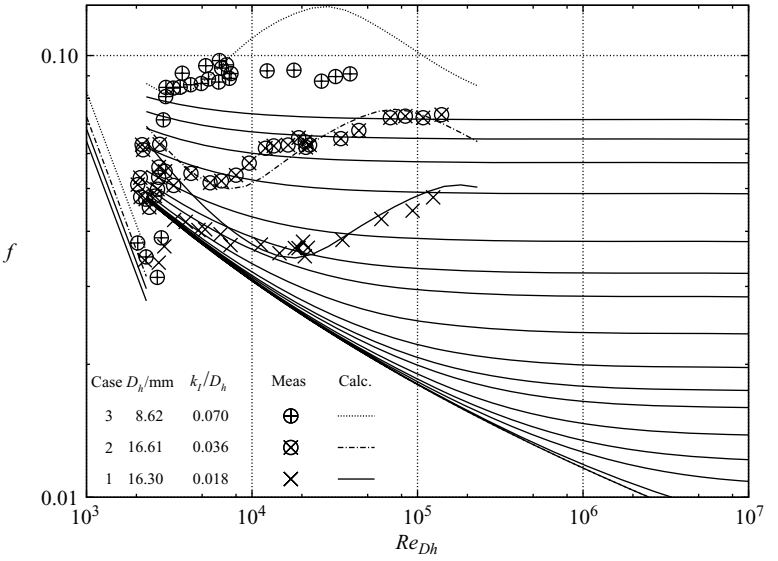

FIGURE 15. Experimental data and numerical results for three different pipes with rough walls and turbulent flow taken from Schiller (1923).

(ii) In Schiller (1923), there are well-documented data of the turbulent flow through pipes with threads taped in along the whole length of the pipe. The geometry of a thread turn is well defined and thus can be incorporated into the dissipation model calculations. From five cases reported, we selected three, since the other two give rise to some doubts concerning the reliability of the data (discussed in Schiller 1923).

Figure 15 shows the friction factor f from the measurements (symbols) compared to our numerical results based on the dissipation model for turbulent flows. Again there is a good accordance, at least for cases 1 and 2. Case 3 was also measured in

the laminar regime (with a good agreement of experimental and theoretical results). There are, however, deviations for Reynolds numbers above 10^4, which could only be understood with more information about the experiments (which are not available).

Altogether, important aspects of the f-distribution for laminar as well as turbulent flows are correctly obtained by the numerical calculations. This underlines the reliability of a theoretical approach based on entropy production considerations.

10. Conclusion

Based on a second law analysis, we could determine friction factors in the laminar as well as in the turbulent range of Reynolds numbers for pipe and channel flows. Thus we were able to provide a theoretical background to the famous Moody chart which so far has been based on experimental results only (at least for its turbulent part).

From our study, the following points are important.

(*a*) The general definition of a friction factor should be based on $\mathrm{d}\varphi/\mathrm{d}x$. Only for steady, fully developed and horizontal flows, can $\mathrm{d}p/\mathrm{d}x$ or τ_w be used instead.

(*b*) Dimensionless groups such as Re_{Dh} and f are defined with a characteristic length and a characteristic velocity. Both these quantities are the characteristic quantities of an equivalent smooth channel. The most reasonable equivalence criterion is a common volume of the real and the equivalent channel.

(*c*) Defining a certain roughness parameter goes hand in hand with a certain concept to account for the influence of surface roughness. The equivalent sand roughness concept is promising; however, it needs a table of correspondence between real and equivalent sand roughness. With our approach, such a table can be determined with high accuracy by calculating the effect of a certain roughness and exactly relating it to the equivalent sand roughness.

(*d*) Laminar flows are modestly affected by wall roughness with a nearly linear increase with respect to a properly defined roughness parameter.

(*e*) If the equivalent sand roughness concept should be extended to cover laminar flows, the table of correspondence cannot be the same for turbulent and for laminar flows.

REFERENCES

Bejan, A. 1996 *Entropy Generation Minimization*. CRS Press, Boca Raton.

Bradshaw, P. 2000 A note on 'critical roughness height' and 'transitional roughness'. *Phys. Fluids* **12**(6), 1611–1614.

Colebrook, C. F. 1939 Turbulent flow in pipes with particular reference to the transition between the smooth and rough pipe laws. *J. Inst. Civil Engrs Lond.* **11**, 133–156.

Croce, G. & D'Agaro, P. 2005 Numerical simulation of roughness effect on microchannel heat transfers and pressure drop in laminar flow. *J. Phys.* D: *Appl. Phys.* **38**, 1518–1530.

Gloss, D., Dittmer, J. & Herwig, H. 2008 A systematic approach to wall roughness effects in laminar channel flows: experiments and modelling. In *Proc. ASME ICNMM2008*.

Herwig, H. & Kautz, C. 2007 *Technische Thermodynamik*. Pearson Studium, München.

Herwig, H. & Kock, F. 2007 Direct and indirect methods of calculating entropy generation rates in turbulent convective heat transfer problems. *Heat Mass Transfer* **43**, 207–215.

Hesselgreaves, J. E. 2000 Rationalisation of second law analysis of heat exchangers. *Intl J. Heat Mass Transfer* **32**, 4189–4204.

Hu, Y., Werner, C. & Li, D. 2004 Influence of the three-dimensional heterogeneous roughness on electrokinetic transport in microchannels. *J. Colloid Interface Sci.* **280**, 527–536.

KANDLIKAR, S. G., SCHMITT, D., CARRANO, A. L. & TAYLOR, J. B. 2005 Characterization of surface roughness effects on pressure drop in single-phase flow in minichannels. *Phys. Fluids* **17**, 1–11.

KLEINSTREUER, C. & KOO, J. 2004 Computational analysis of wall roughness effects for liquid flow in micro-conduits. *Trans. ASME* I: *J. Fluids Engng* **126**, 1–9.

KOCK, F. & HERWIG, H. 2004 Local entropy production in turbulent shear flows: a high Reynolds number model with wall functions. *Intl J. Heat Mass Transfer* **47**, 2205–2215.

LANGELANDSVIK, L. I., KUNKEL, G. J. & SMITS, A. J. 2008 Flow in a commercial steel pipe. *J. Fluid Mech.* **595**, 323–339.

MATHIEU, J. & SCOTT, J. 2000 *An Introduction to Turbulent Flow*. Cambridge University Press.

MOODY, L. F. 1944 Friction factors for pipe flow. *Trans. ASME* **66**, 671–684.

MUNSON, B. R., YOUNG, D. F. & OKIISHI, T. H. 2005 *Fundamentals of Fluid Mechanics*, 5th edn. John Wiley.

NIKURADSE, J. 1930 Turbulente Strömung in nicht kreisförmigen Rohren. *Ing.-Arch.* **1**, 306–332.

NIKURADSE, J. 1933 Strömungsgesetze in rauhen Rohren. In *Forschungsheft*. VDI, Düsseldorf.

PERRY, A. E., SCHOFIELD, W. H. & JOUBERT, P. N. 1969 Rough wall turbulent boundary layers. *J. Fluid Mech.* **37**, 383–413.

ROSEN, M. A. 1998 Second-law analysis: approaches and implications. *Intl J. Energy Res.* **23**, 415–429.

SCHILLER, L. 1923 Über den Strömungswiderstand von Rohren verschiedenen Querschnitts- und Rauhigkeitsgrades. *Z. Angew. Math. Mech.* **3**, 2–13.

SCHLICHTING, H. 1965 *Grenzschicht-Theorie*, 5th edn. G. Braun, Karlsruhe.

SCHLICHTING, H. & GERSTEN, K. 2000 *Boundary Layer Theory*, 8th edn. Springer.

SHOCKLING, M. A., ALLEN, J. J. & SMITS, A. J. 2006 Roughness effects in turbulent pipe flows. *J. Fluid Mech.* **564**, 267–285.

SLETFJERDING, E., GUDMUNDSSON, J. & SJØEN, K. 1998 Flow experiments with high pressure natural gas in coated and plain pipes. In *Proc. 1998 PSIG Conf. Denver, Colorado*.

STREETER, V. L. 1936 Frictional resistance in artificially roughened pipes. *Trans. ASCE* **101**, 681–704.

WANG, S. P., CHEN, Q. L., YIN, Q. H. & HUA, B. 2003 Exergy destruction due to mean flow and fluctuating motion in incompressible turbulent flows through a tube. *Energy* **28**, 809–823.

WHITE, F. M. 2005 *Viscous Fluid Flow*, 3rd edn. McGraw-Hill.

YAKHOT, V. & ORSZAG, S. A. 1986 Renormalization group analysis of turbulence. I. Basic theory. *J. Sci. Comput.* **1**(1).